Title

Structure and Chemical Composition of a Supported Pt-Ru Electrocatalyst for Methanol Oxidation

Authors

Radmilovic, V.
Gasteiger, H.A.
Ross, P.N.

Publication Date

1994-09-01

LBL-36167
UC-404
Preprint

Lawrence Berkeley Laboratory
UNIVERSITY OF CALIFORNIA

Materials Sciences Division
National Center for Electron Microscopy

Submitted to Journal of Catalysis

Structure and Chemical Composition of a Supported Pt-Ru Electrocatalyst for Methanol Oxidation

V. Radmilovic, H.A. Gasteiger, and P.N. Ross Jr.

September 1994

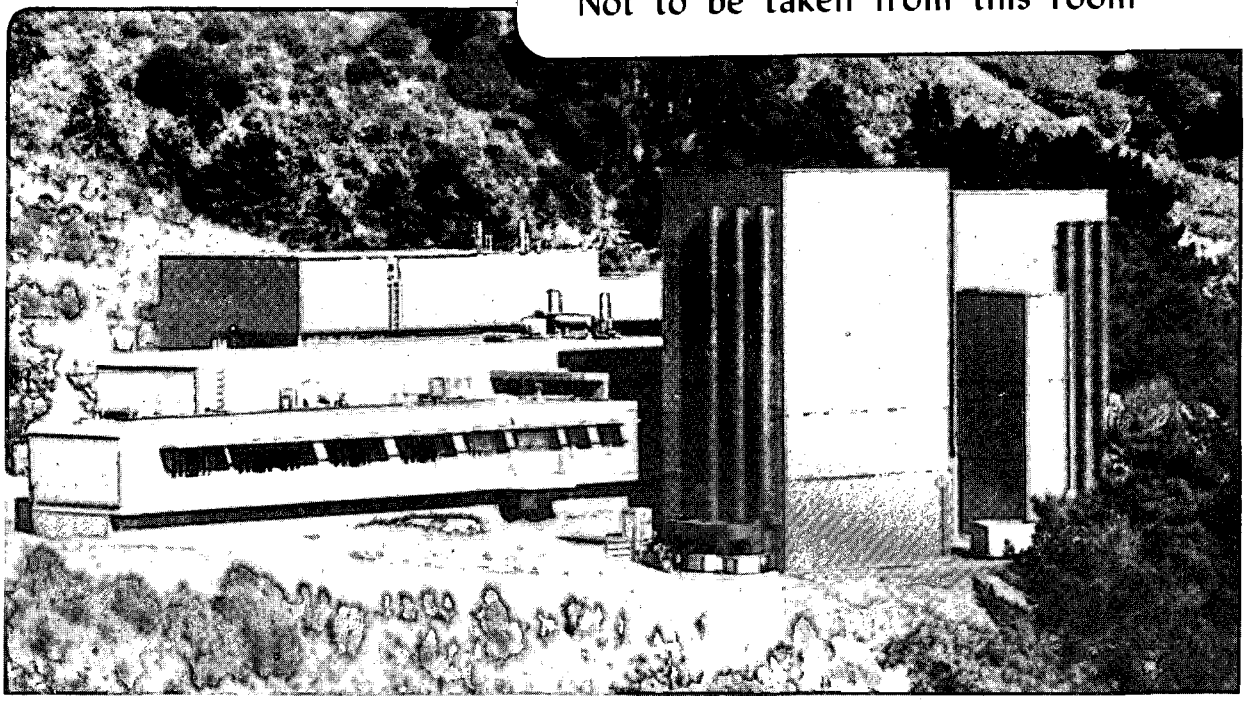

Prepared for the U.S. Department of Energy under Contract Number DE-AC03-76SF00098

DISCLAIMER

LBL-36167

Structure and Chemical Composition of a Supported Pt-Ru Electrocatalyst for Methanol Oxidation

V. Radmilovic*, H.A. Gasteiger, and P.N. Ross Jr.

Materials Sciences Division
Lawrence Berkeley Laboratory
University of California, Berkeley, CA 94720

*Permanent address: University of Belgrade
Department of Physical Metallurgy
Karnegijeva 4. P.P. 494
11001 Belgrade, Yugoslavia

Journal of Catalysis (to be submitted)

This work was supported in part by the Assitant Secretary for Energy Efficiency and Renewable Energy, Office of Transportation Technologies, Electric & Hybrid Propulsion Division and by the Director, Office of Energy Research, Office of Basic Energy Sciences, Materials Science Division of the U.S. Department of Energy under Contract No. DE-AC03-76SF00098.

to be submitted to *Journal of Catalysis* 09/21/94

Structure and Chemical Composition of a Supported Pt-Ru Electrocatalyst for Methanol Oxidation

V. Radmilović*, H.A. Gasteiger, and P.N. Ross (Jr.)

National Center for Electron Microscopy, and

Material Science Division,

Lawrence Berkeley Laboratory,

Berkeley, CA 94720

Abstract

High resolution electron microscopy (HREM) and X-ray microchemical analysis (EDS) were used to characterized composition, size, distribution and morphology of Pt-Ru particles with nominal Pt:Ru ratio 1:1 and 3:1, supported on carbon black. The particles are predominantly single nanocrystals with diameters in the order of 2.0 to 2.5 nm. Occasionally, twinned particles are also observed. All investigated particles represent solid solutions of Pt and Ru with compositions very close to the nominal one. Based on two-dimensional projection in high resolution images, it is suggested that the well resolved particles are of cubooctahedral shape. In addition to {200} and {111} facets, {113} facets are also observed.

* Permanent address: University of Belgrade, Department of Physical Metallurgy, Karnegijeva 4, P.P. 494, 11001 Belgrade, Yugoslavia.

1. INTRODUCTION

Bimetallic alloy particles supported on high-surface area carbon find widespread application as electrode materials. Of particular interest are platinum-ruthenium alloys used for the electrooxidation of methanol at the anode of low temperature fuel cells [*e.g.*, 1, 2, 3]. The choice of precursor molecules and formation conditions in the preparation of bimetallic Pt-Ru catalysts strongly affects the dispersion and the compositional homogeneity of the alloy clusters [4, 5], both of which are important factors in determining their electrocatalytic activity towards methanol oxidation. Since the catalysis for this reaction is governed by the bifunctional character displayed by Pt-Ru alloy electrodes [6], it follows that separate particles of the pure elements are relatively inactive compared to clusters consisting of a true Pt-Ru alloy. Therefore, it is clearly of importance to verify the desired compositional homogeneity of the supported bimetallic particles, *i.e.*, to assess the extent of alloy formation. Furthermore, as the utilization of the precious metals is inversely related to the particle size, their dispersion should be maximized and state-of-the-art Pt-on-carbon fuel cell catalysts usually range from 80 [2] to 100 m^2/g_{metal} [7], corresponding to particles in the range of 1.5 to 3 nm in diameter. The focus of the present work is to examine a commercially available carbon supported bimetallic Pt-Ru catalyst [8] in terms of particle size and the completeness of alloy formation using high resolution electron microscopy (HREM), electron and X-ray diffraction, and microchemical analysis by energy dispersive X-ray spectroscopy (EDS).

The nanosize of these particles presents challenges to their microstructural characterization. Many of these challenges can be addressed by using transmission electron microscopy, especially for lattice structure characterization by high resolution electron microscopy, including the presence of defects as dislocations, twins, etc. The advantage of the application of TEM in catalyst characterization is described in several

recently published review articles [9, 10, 11]. HREM has been extensively used to determine faceting planes, i.e. its geometric shape, the presence of surface steps, surface roughness, as well as size and distribution of the Pt-Ru particles. Weak beam dark field imaging (WBDF) has not been used because of its well known limitations if the particle size is less than 10 nm [12, 13, 14, 11].

2. EXPERIMENTAL

2.1. HREM

In this investigation two Pt-Ru catalysts denoted as #1 (Pt:Ru=1:1) and #2 (Pt:Ru=3:1) supported on carbon black were examined [8]. Specimens were prepared for transmission electron microscopy examination by ultrasonically suspending the catalyst powders in ethanol. A drop of suspension was then applied onto clean holey carbon grids and dried in air; in a second set of experiments, the catalyst powder was pressed onto copper grids. Samples were examined using the Topcon O2B and JEOL ARM high resolution electron microscopes at NCEM [15] as well as a JEOL 200CX analytical electron microscope. The particle shapes were determined by real space crystallography using high resolution electron microscopy images taken from the particles near or on the edge of the carbon black substrate. In order to get information about the overall distribution of Pt-Ru particles, dark-field imaging was also utilized.

To avoid contamination during energy dispersive X-ray spectroscopy (EDS) analysis, the microchemical analysis was performed at -160^{o}C using a cold stage beryllium holder. This was found to be essential because of the time required for statistically significant spectral acquisition from samples with a particle size on the order of $\approx$2 nm (or particle clusters) using a 10 nm electron beam. The fluorescence effect can be neglected [16]. Local structural information from single particles were obtained by digitized optical diffraction.

2.2. X-ray diffraction

X-ray diffraction data of samples #1 (Pt:Ru=1:1) and #2 (Pt:Ru=3:1) were acquired with a Siemens powder diffractometer (model D500). The angular resolution in the 2θ-scans was 0.05° for the wide-angle 2θ-scans, and 0.02° for detailed scans about the (220) peak of the fcc (face centered cubic) Pt-Ru alloy face. Spectral contributions of the copper $K\alpha_2$ line were subtracted prior to data analysis by a Rachinger algorithm correction [17], resulting in a symmetrical peak for the (220) face. The instrumental line broadening was measured under the same conditions on a homogenized Pt-Ru alloy sample with 30 atomic% Ru (for a description of the bulk alloy preparation see Reference 18), yielding a full width at half maximum (FWHM) in the 2θ-scan, $B_{(2\theta)}$, of 0.5°, thus marking the upper bound for the instrumental line broadening.

3. RESULTS AND DISCUSSION

3.1. X-ray diffraction data analysis

3.1.1. Wide-angle scans

Figures 1 and 2 show the X-ray diffraction patterns measured on the catalyst powders with Pt:Ru ratios of 3:1 and 1:1, respectively. Both samples exhibit only the characteristic diffraction peaks (marked in the figures) of the fcc Pt-Ru bulk alloys with a Ru concentration of less than ≈62 atomic% [18]. The merging of the closely spaced (331) and the (420) peak ($\Delta_{(2\theta)}\approx5°$) can be accounted for by particle size broadening, which increases with $1/\cos\theta$ [19], effecting a $B_{(2\theta)}$ of ≈6-8° based on the width of the (220) peak and the particle sizes measured as described below. It is important to note that no diffraction peaks appear which would indicate the presence of an either pure Ru or Ru-rich hcp phase, so that it may be concluded that the catalysts are composed only of fcc Pt-Ru alloy particles. Furthermore, the absence of any superimposed sharp diffraction peaks indicates a unimodal particle distribution. This is in contrast to the report by Del

Angel *et al* [16] of both Pt-Ru clusters (< 5 nm) and large (> 50 nm) particles of pure Ru for a Pt-Ru catalyst supported on silica. This result re-emphasizes the importance of matching the preparation chemistry with the surface chemistry of the support to achieve optimal bimetallic dispersion.

At the low 2θ-range, in the vicinity of the (111) fcc diffraction peak of the alloys one can observe the strong background from the two-dimensional (10) reflection from individual carbon layers in the carbon black, following the analysis by Warren [20]. The other two characteristic diffraction peaks for the carbon black in the recorded 2θ-range are the (004) reflection at ≈55° and the (11) two-dimensional reflection at ≈78°. The latter is overlapping with the (311) diffraction of the fcc Pt-Ru alloy. Therefore, in order to assess both the particle size of the bimetallic clusters on the carbon support as well as to verify the high degree of alloy formation, *i.e.*, compositional homogeneity, we analyzed the (220) reflections in detail, the angular position of which is in a range where the diffraction spectrum of the carbon support only contributes in terms of a linear background.

3.1.2. (220) diffraction peaks

Particle size broadening, after subtraction of contributions from Cu $K\alpha_2$, should result in a gaussian line shape of the (220) reflection, convoluted with a linear background from the carbon support as outlined above. We therefore fitted the X-ray diffraction data to a gaussian on a linear background, with the constraint that the slope be identical for both of the investigated samples, since it should be characteristic to the carbon itself. The pertinent results of a least squares regression are summarized in Table 1 and are illustrated in the inserts of Figures 1 and 2. In general, the measured line broadening represents a convolution of the instrument broadening with the particle size broadening. As mentioned in Section 2, the instrumental broadening, $B_{(2\theta)instr.}$ is less than

.9 mrad ($\lesssim 0.5°$) and its convolution with the measured FWHM in Table 1, $B_{(2\theta)measured}$, changes the FWHM for the true particle size broadening only by ≈1%:

$$B_{(2\theta)particle} = \sqrt{B_{(2\theta)measured} - B_{(2\theta)instr.}} \quad (1)$$

This change is small compared to the ≈5% uncertainty in the measured $B_{(2\theta)}$ and will thus be neglected. Similarly, potential peak broadening induced by crystal strain is negligible compared to particle size broadening effects. Therefore, the average particle size, L, may be estimated from the parameters listed in Table 1 according to the Scherrer formula [19]:

$$L = \frac{0.9\,\lambda_{K\alpha_1}}{B_{(2\theta)}\cos\theta_{max}} \quad (2)$$

where $\lambda_{K\alpha_1}$ is 1.54056 Å, and $B_{(2\theta)}$ is in radians. Hence, the average particle for the two catalysts with a Pt:Ru ratio of 3:1 and 1:1 is 2.3 and 1.9 nm, respectively, with an estimated error of ±6% based on the error bounds of the fitted parameters in Table 1 and assuming a unimodal particle size distribution (see Figure 5).

The fcc lattice parameters for single-phase Pt-Ru bulk alloys (see Reference 18) with Ru concentrations of less than 60 atomic% are shown in Figure 3, closely following a Vegard's Law relation, in excellent agreement with a previous study on cold-rolled alloy sheets [21]. Lattice parameters can be evaluated from the angular position of the peak maxima (θ_{max} , Table 1):

$$a_{fcc} = \frac{\sqrt{2}\,\lambda_{K\alpha_1}}{\sin\theta_{max}} \quad (3)$$

yielding 0.3898 nm for sample #2 (Pt:Ru=3:1), and 0.3884 nm for sample #1 (Pt:Ru=1:1). The estimated error of ±0.5% for this measurement (indicated by the error bars in Figure 3) is mainly due to the large penetration depth of the X-rays through the carbon matrix with its low absorption coefficient [19], effecting diffraction throughout

the entire thickness of the sample powder in the holder (≈1 mm). Even though this large error does not allow for the assessment of the sample composition from measured lattice parameter values, the decrease in the lattice parameter with increasing Ru concentration does lend further support to the above idea that the supported bimetallic catalysts are indeed a solid solution of Pt and Ru, rather than being a physical mixture of particles of the two metals.

3.2. High resolution electron microscopy

Typical conventional TEM bright field and dark field images of the Pt-Ru catalysts are shown in Figures 4a and b. The dark field image is taken using the (002) diffraction ring (Figure 4c). The dark field images indicate qualitatively that the particle size is relatively small, *e.g.*, < 10 nm. Both images show that the distribution of the metal particles on the carbon support is reasonably uniform, an especially important characteristic for an electrocatalyst [22]. The relatively strong intensity of the (111) diffraction ring might be an indication of a preferred orientation of the metal particles with respect to the carbon substrate

Both the 1:1 and 3:1 catalyst have similar particle size and morphology. Histograms of the particle size distributions in the two catalysts are shown in Figure 5. These histograms include analyses of several different regions in the same catalyst, including some regions where the metal particle distribution was less uniform than in Figure 4, *e.g.*, much more concentrated. Nonetheless, the particle size distribution is remarkably uniform, with the average particle size being *ca.* 2 nm for both catalysts in good agreement with the XRD measurements (Section 3.1).

Two-dimensional projections, such as those in Figure 6, give the impression of spherical or elliptical shapes, as opposed to faceted shapes such as cubooctahedral-octahedral. However, apparent rounding of particles can be caused by two effects: due to the inclination of the particles from the low index zone axis, faceted corners appear to be

slightly curved; even when particles are aligned along a low index zone axis they can appear to be spherical because of interference from the carbon substrate and confusing contrast (*e.g.*, as in [23]) that obscures sharp edges and corners. The latter effect can be avoided by analyzing particles close to the edge of the carbon support, such as those shown in Figure 7. Detailed analyses of particles on or close to the edges of the carbon support show they are faceted on (111) and (200) planes, characteristic of fcc asymmetric or symmetric cubooctahedral nanocrystals. However, the majority of the particles in the catalysts are not conveniently located on edges of the carbon substrate, so that analysis of only these particles may not be representative of the catalyst as a whole. The contrast problem with particles on the thick regions of the carbon were reduced by use Fourier filtering, which can remove much of the contribution from the incoherent scattering of electrons from the amorphous carbon. As shown in Figure 8, Fourier filtered images from particles in the interior of catalyst still reveal faceted shapes, typically cubo-octohedral.

The nominally 0.2 nm and 0.23 nm spacings of the (002) and (111) planes, respectively, of the fcc lattice of a typical faceted particle is indicated by the arrows in Figure 7b. More accurate measurements of the lattice spacing were made using a Cu grid as an internal calibration (Figure 9a). Lattice spacings measured on different particles in the same catalyst varied by about ±0.4 %. We attribute this variation to the effect of tilt on measured interplanar spacing, consistent with the calculations of Malm and O'Keefe [24]. A typical result is shown in Figure 9b for a single particle in the nominally 3:1 catalyst. The lattice constant from the spacing of the (111) planes is 0.3902 ± 0.0015 nm in reasonable agreement for the value for the 3:1 bulk alloy (Figure 3, 0.3895 nm) and again in close agreement with the XRD measurements. However, the lattice constant measurement from interplanar spacing does not have sufficient accuracy to determine compositional variations between particles beyond extremes, *e.g.*, pure Ru and Ru-rich

phases, since ±1 % covers the whole range of lattice parameters between pure Pt and 1:1 Pt:Ru (Figure 3).

The electron diffraction patterns, including the single-particle micro-diffraction pattern shown in Figure 10, were characteristic of only Pt-rich fcc phases. The beam size was 10 nm, well above the average particle size, so that observed additional weak diffraction spots (other than 112 spots) probably derive from the partial sampling of neighboring particles. No pure Ru or Ru-rich hcp particles were observed. The EDS analyses, summarized in Table 2, show that regardless of the beam size and/or particle size(s) under the beam, the Pt:Ru ratio was always the same and in reasonable agreement with the nominal composition of the catalyst, *i.e.*, 1:1 and 3:1. All of the microscopic characterization indicates that essentially all of the metal particles are bimetallic nanocrystals having nearly identical composition and approximately the same size.

Occasionally, particles having {113} facets and twinned particles were also observed. Although these features were atypical, their existence in these catalysts is noteworthy, since we have never seen either twins or {113} facets in pure Pt catalysts on the same support pre-treated in the same way. An example of the simultaneous occurrence of both in the same particle is shown in Figure 11. This particle has the same (111) twinning plane as in other fcc metals. The almost perfect {113} facet does not appear to be accompanied by any relaxation in the interatomic spacing near the surface, as might occur with a surface enriched in one element relative to the bulk, but as we stated above the change in interplanar spacing in this alloy is too small to be observed by lattice imaging. The fact that these unusual features are correlated to the existence of Ru atoms in the particles suggests that their occurrence may be related also to the effect of Ru on the bulk lattice, *e.g.*, residual stress due to the expected composition gradient between the surface and the bulk [18].

The investigated Pt-Ru particles supported on carbon black were observed to be relatively stable under irradiation, and a shape change under illumination has not been

observed, as reported for ultrafine gold particles, supported on amorphous Si and SiO_2 [25], MgO [26], or TiO_2 substrate [27], and in several other pure metals supported on carbon black [28, 29], including Pt [12]. Marks and coworkers [30] suggested that the reason for this behavior could be a relatively small activation barrier (a few electron volts) for transformations between different shapes compared to the energy deposited by the electron beam (100 to 1000 eV). This suggests that stability of Pt-Ru particles can be related to their bimetallic nature or the presence of Ru in Pt based solid solution. Since our observation indicates higher stability of Pt-Ru particles than pure Pt, it suggests that Ru possibly increases the activation barrier for shape transformation.

Finally, we consider the very important question, from a catalytic standpoint, of the surface composition of the particles. In bulk Pt-Ru alloys of 1:1 and 3:1 composition, the clean annealed surface is considerably enriched in Pt [18] due to the lower surface tension of Pt and a nearly zero heat of mixing [31]. This enrichment has a profound effect on the kinetics of methanol electrooxidation [6]. One might expect to be able to observe surface enrichment by HREM by the measurement of the surface relaxation in individual particles, especially particles on the very edge of the carbon substrate. Surface relaxation measurements are not straightforward, as pointed out by Gibson [32] in his discussion of the measurements of the surface relaxation on gold particles by Marks and Heine [33]. There is also a contribution of the sample tilt and uncertainties in the exact direction of the surface normal that can be misinterpreted as part of the surface relaxation, as shown by Malm and O'Keefe [24]. According to their calculations [24], the errors in the measurement of interplanar relaxation in high resolution images are on the order of a few %, and can be as high as 10 %. Since the surface relaxation even for a pure Pt surface layer on top of an alloy bulk lattice would only be *ca.* 2 %, we concluded it was not possible to make any determinations about surface composition in these catalysts.

5. CONCLUSIONS

Based on the analysis of the Pt-Ru electrocatalysts supported on carbon black using the combination of x-ray diffraction and high resolution and analytical electron microscopy, we made the following conclusions:

1.) The presence of Ru in the catalyst appeared to have relatively little effect on the resulting particle size, with the average particle size being *ca.* 2 - 3 nm for both the 3:1 and 1:1 (Pt:Ru) catalysts, which is also about the same particle size as for pure Pt particles on the same support. The particle size distribution for 90 % of the particles was ±0.5 nm and ±0.2 nm for the catalysts with a Pt:Ru ratio of 3:1 and 1:1, respectively.

2.) The particles are essentially uniform in composition, having the same composition as the nominal composition of the bulk catalyst. Thus, the particles are all fcc alloy nanocrystals of Ru in a Pt solid solution. We were unable to determine if there is any surface segregation (enrichment in Pt) in the individual nanocrystals.

3.) The majority of the particles are truncated by the (111) and (200) crystallographic planes and are cubooctahedral in shape, as observed in pure Pt and in many other fcc metal nanocrystals. However, occasionally {113} type facets that are not typical of fcc nanocrystals were observed, and occasionally twinned particles were also observed, which is not generally the case for pure Pt particles on the same carbon support.

ACKNOWLEDGMENT

This work was supported by the Assistant Secretary for Energy Efficiency and Renewable Energy, Office of Transportation Technologies, Electric & Hybrid Propulsion Division, and by the Director, Office of Energy Research, Office of Basic Energy Sciences, Materials Sciences Division of the U.S. Department of Energy under contract No. DE-AC03-76SF00098.

REFERENCES

[1] Cameron, D.S., Hards, G.A., and Thompsett, D., *in* "Proceedings of the Workshop on Direct Methanol-Air Fuel Cells" (A.R. Landgrebe, R.K. Sen and D.J. Wheeler, Eds.), Vol. 92-14, p. 10. The Electrochemical Society, Pennington, N.J., 1992.

[2] Watanabe, M., Uchida M., and Motoo, S., *J. Electroanal. Chem.* **229**, 395 (1987).

[3] Wasmus, S., and Vielstich, W., *J. Appl. Electrochem.* **23**, 120 (1993).

[4] Miura, H., Suzuki, T., Ushikubo, Y., Sugiyama, K., Matsuda, T., and Gonzales, R.D., *J. Catal.* **85**, 331 (1984).

[5] Alerasool, S., and Gonzales, R.D., *J. Catal.* **124**, 204 (1990).

[6] Gasteiger, H.A., Marković, N., Ross (Jr.), P.N., and Cairns, E.J., *J. Phys. Chem.* **97**, 12020 (1993).

[7] Wilson, M.S., Garzon, F.H., Sickafus, K.E., and Gottesfeld, S., *J. Electrochem. Soc.* **140**, 2872 (1993).

[8] The two investigated catalyst samples were provided by E-TEK Inc. (Natick, MA) and had a metal loading of 20 wt.% on Vulcan XC-72 with atomic ratios of Pt to Ru of 1:1, and 3:1, respectively. The catalysts were prepared by co-impregnation of

the carbon support using a proprietary method. Prior to our analysis, the catalyst was reduced in flowing H_2 at 250°C.

[9] Datye, A.K., and Smith, D.J., *Catal. Rev.-Sci. Eng.* **34**, 129 (1992).

[10] Yacaman, M.J., and Avalos-Borja, M., *Catal. Rev.-Sci. Eng.* **34**, 55 (1992).

[11] Popa, H., *Catal. Rev.-Sci. Eng.* **35**, 359 (1993).

[12] Sattler, M.L., and Ross, P.N., *Ultramicroscopy* **20**, 21(1986).

[13] Smith, D.J., and Marks, L.D., *Ultramicroscopy* **16**, 101 (1985).

[14] Yacaman, M.J., and Dominguez, J.M., *J. of Catalysis* **64**, 213 (1980).

[15] National Center for Electron Microscopy, Lawrence Berkeley Laboratory, Berkeley, CA 94720.

[16] Del Angel, G., Alerasool, S., Domingues, J. M., Gonzales, R. D., Gomez, R., *Surface Science* **224**, 407 (1989).

[17] The Rachinger correction was carried out with the instrument controlling software (Diffrac-AT v.3.1).

[18] Gasteiger, H.A., Ross, P.N. (Jr.), and Cairns, E.J., *Surf. Sci.* **293**, 67 (1993).

[19] Warren, B.E. "X-Ray Diffraction." Addison-Wesley Publishing Company, Reading (Massachusetts), 1969.

[20] Warren, B.E. *in* "Proceedings of the First and Second Conferences on Carbon" (held at the University of Buffalo, N.Y.), p. 49. Waverly Press, Baltimore, 1956.

[21] Binder, H., Köhling, A., and Sandstede, G., *in* "From Electrocatalysis to Fuel Cells" (G. Sandstede, Ed.), p. 43. University of Washington Press, Seattle, 1972.

[22] Kunz, H.R., Gruver, G., *J. Electrochem. Soc.* **122**, 1279 (1975).

[23] Chojanacki, T., Krause, K., and Schmidt, L.D., *J. of Catalysis* **128**, 161 (1991).

[24] Malm, J.-O., and O'Keefe, M.A., *Proc. EMSA* (1993), p. 974.

[25] Iijima, S., and Ichihashi, T., *Physical Rev. Letters* **56**, 616 (1986).

[26] Marks, L.D., and Ajayan, P.M., *Physical Rev. Letters* **63**, 279 (1989).

[27] Fuchs, G., Neiman, D., and Poppa, H., *Langmuir* **7**, 2853 (1991).

[28] Yao, M.-H., Smith, D.J., and Datye, A.K., *Ultramicroscopy* **52**, 282 (1993).

[29] Dahmen, U., *MRS Bulletin* **24**, 341 (1994).

[30] Dundurs, J., Marks, L.D., and Ajayan, P.M., *Phil. Mag. A* **57**, 605 (1988).

[31] Miedema, A.R., *Philips Tech. Rev.* **36**, 217 (1976).

[32] Gibson, J.M., *Physical Rev. Letters* **53**, 1859 (1984).

[33] Marks, L.D., and Heine, V., *Physical Rev. Letters* **52**, 656 (1984).

Table 1. Peak position and FWHM derived from a five parameter least squares fit of the (220) diffraction data to a gaussian line shape with linear background; the resulting curves are plotted in the inserts of Figures 1 and 2. The overall regression coefficient, r^2, is 0.949, and the given errors represent the 99% confidence limits. The slope of the background was constrained to be identical for both samples.

	Pt:Ru = 3:1 (see Fig. 1)	Pt:Ru = 1:1 (see Fig. 2)
$2\theta_{max}$ in degrees	67.96±0.05	68.24±0.08
$B_{(2\theta)}$ in mrad	71.0±2.6	86.4±4.8

Table 2. X-Ray Microanalysis of investigated Pt-Ru particles [at. %].

Analysis	Ru	Pt	Beam [nm]	Remarks
Catalyst # 2 (nominal ratio Pt:Ru=3:1)				
1	25.1	74.9	10	particle 3nm
2	24.8	75.2	10	bulk
3	24.7	75.3	10	bulk
4	24.7	75.3	30	cluster 30nm
Average	24.8	75.2		
Catalyst # 1 (nominal ratio Pt:Ru=1:1)				
1	49.2	50.8	20	cluster 50nm
2	49.0	51.0	20	cluster 60 nm
3	52.1	47.9	20	cluster 10 nm
4	52.1	47.9	20	bulk
5	49.2	50.8	20	cluster 30 nm
6	52.9	47.1	20	cluster 20 nm
Average	50.75	49.25		

FIGURE CAPTIONS

Figure 1. X-ray diffraction pattern of a carbon-supported Pt-Ru catalyst (see Reference 8) with an atomic ratio of Pt:Ru of 3:1. Diffraction peaks in the wide-angle 2θ-scan are indicated in the figure. The insert shows the detailed scan about the (220) fcc reflection of the Pt-Ru alloy clusters: circles represent raw data; (——) least squares fit to a Gaussian with linear background.

Figure 2. X-ray diffraction pattern of a carbon-supported Pt-Ru catalyst (see Reference 8) with an atomic ratio of Pt:Ru of 1:1. Diffraction peaks in the wide-angle 2θ-scan are indicated in the figure. The insert shows the detailed scan about the (220) fcc reflection of the Pt-Ru alloy clusters: circles represent raw data; (——) least squares fit to a Gaussian with linear background.

Figure 3. Fcc lattice parameters for Pt-Ru bulk alloys *versus* the atomic fraction of Pt (see Reference 18). The linear regression fit to Vegard's Law is shown in the figure as well as lattice parameters of carbon supported Pt-Ru particles measured by XRD and HREM.

Figure 4. A typical conventional TEM bright field **(a)** and dark field **(b)** image of investigated Pt-Ru catalyst; the dark field is taken using 111 ring intensity (see insert).

Figure 5. Histograms of the Pt-Ru particles size distribution in the catalysts with Pt:Ru ratios 3:1 **(a)** and 1:1 **(b)**.

Figure 6. (a) Low magnification HREM micrograph of Pt-Ru catalysts supported on black carbon: **(a)** Pt:Ru=3:1; **(b)** Pt:Ru=1:1.

Figure 7. HREM micrograph of a carbon supported Pt-Ru particle (Pt:Ru=3:1) on the edge of the carbon support: **(a)** unfiltered image of asymmetric cubooctahedral particle (insert: 110 microdiffraction pattern); **(b)** Fourier filtered image.

Figure 8. HREM micrograph of carbon a supported Pt-Ru particle (Pt:Ru=3:1) in the interior region of the catalyst. **Left:** unfiltered image of symmetric cubooctahedral particle; **center:** microdiffraction pattern); **right:** Fourier filtered image.

Figure 9. Digitized selected area electron diffraction pattern from the catalyst containing Pt and Ru in the ratio 3:1 Obtained at 800 kV in the ARM electron microscope. **(a)** calibration of the camera constant using the Cu grid; **(b)** microdiffraction from the catalyst sample.

Figure 10. Microdiffraction of small Pt-Ru (3:1 ratio) particle in [112] zone axis obtained at 200 kV in the JEM-200CX electron microscope (left); calculated fcc diffraction pattern for the [112] zone axis (right).

Figure 11. High resolution electron micrograph of a twinned particle found in Pt-Ru (3:1) catalyst: **(a)** -70 nm defocus setting; **(b)** -80 nm defocus setting. {113}, {200} facets and the twinning plane are indicated in the figure.

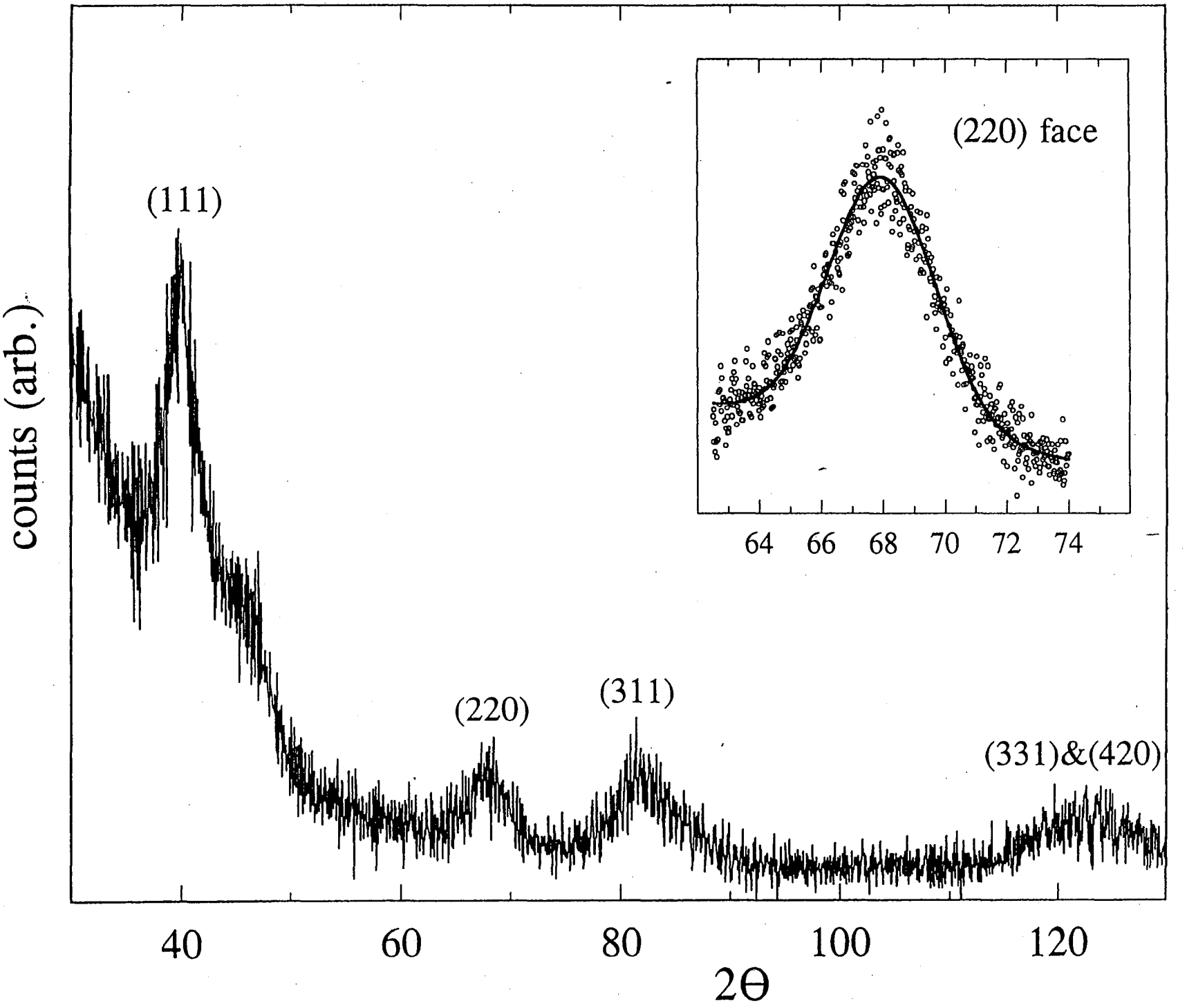

Radmilovic et al, Figure 1

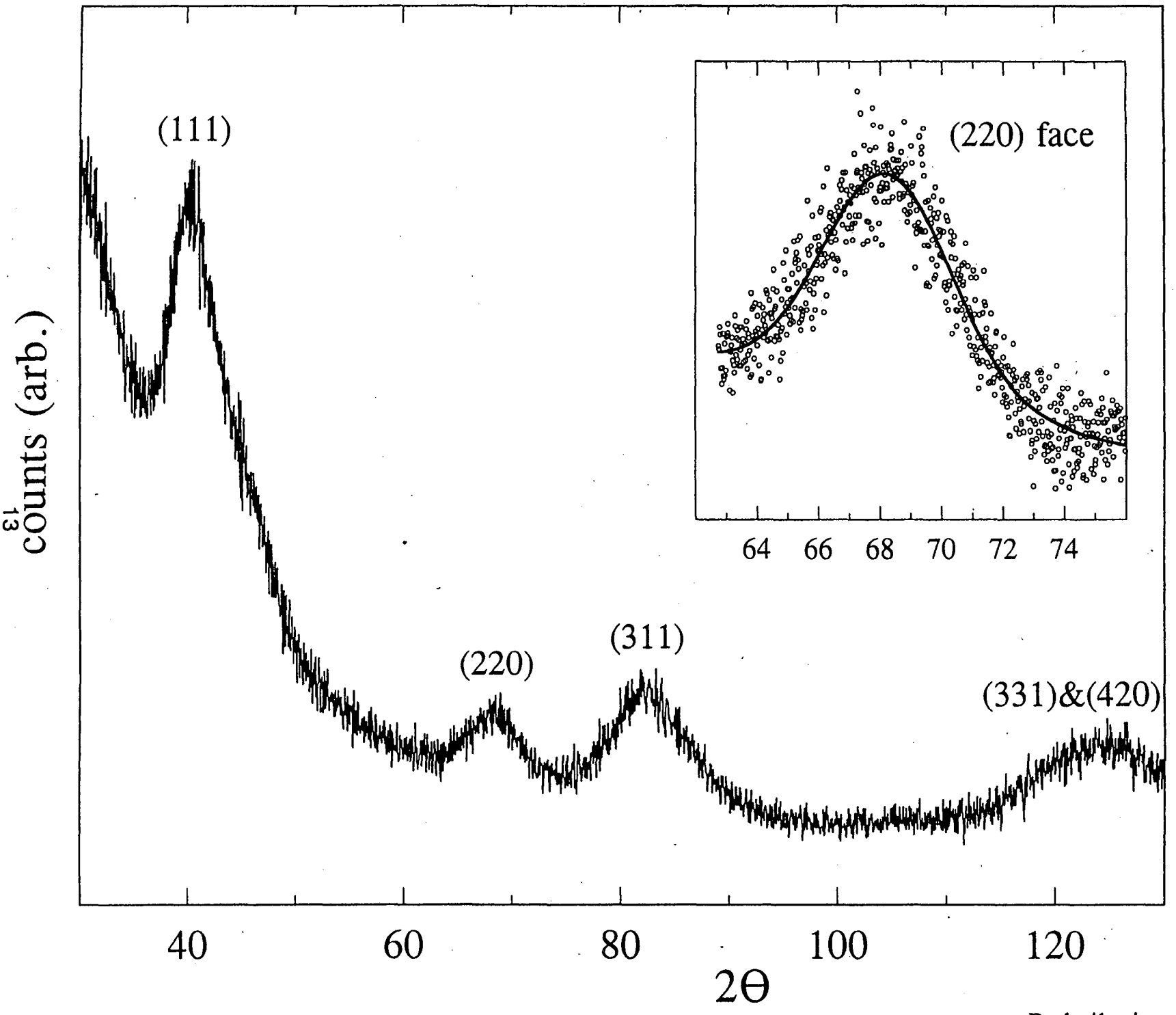

Radmilovic et al, Figure 2

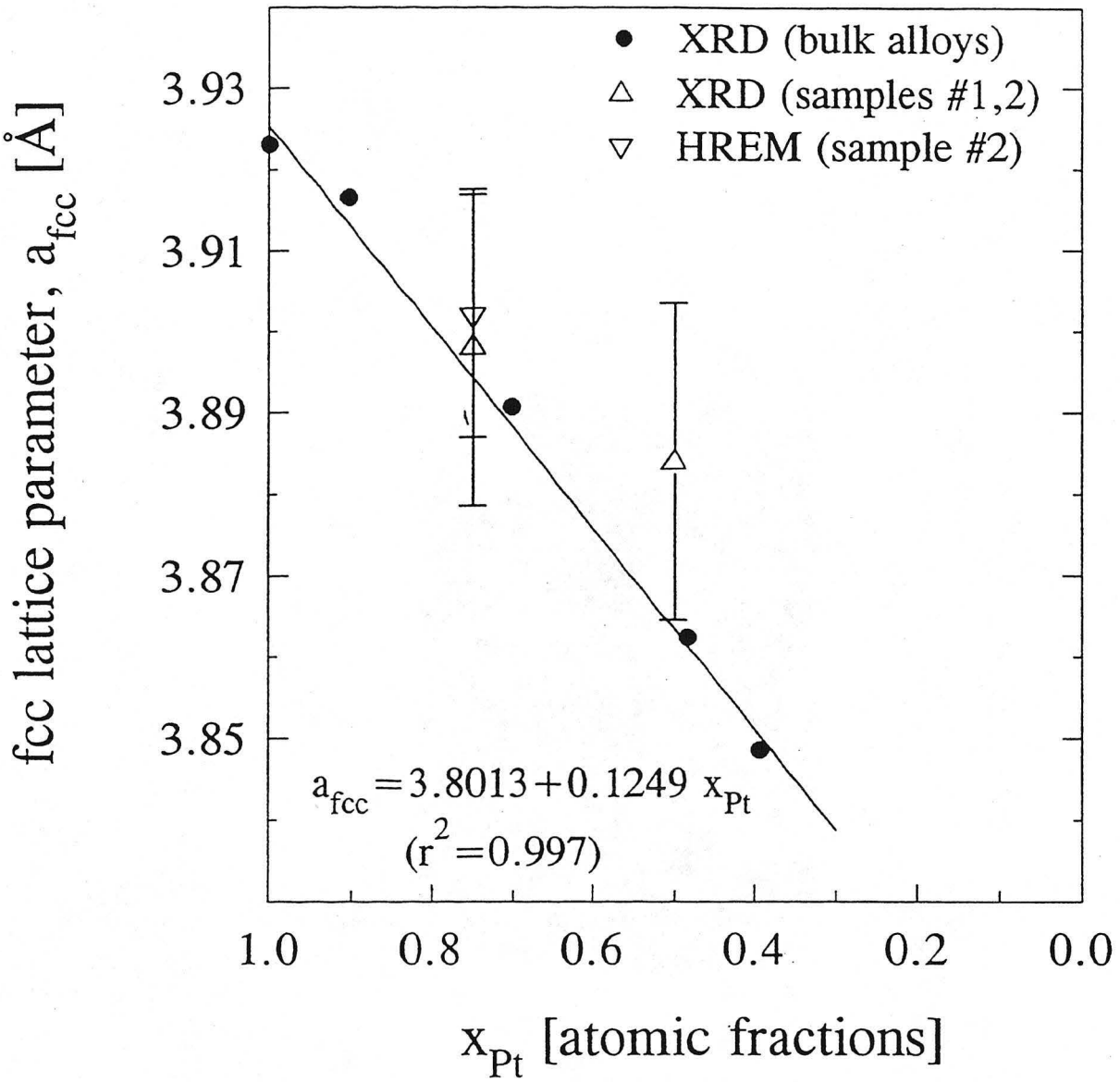

Radmilovic et al, Figure 3

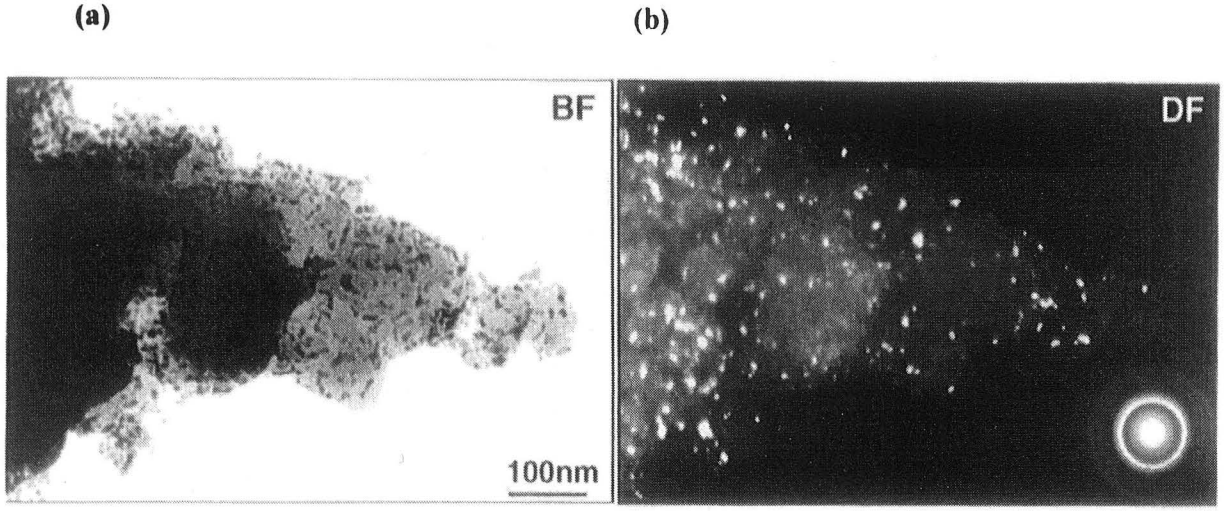

Radmilivić *et al*, Figure 4

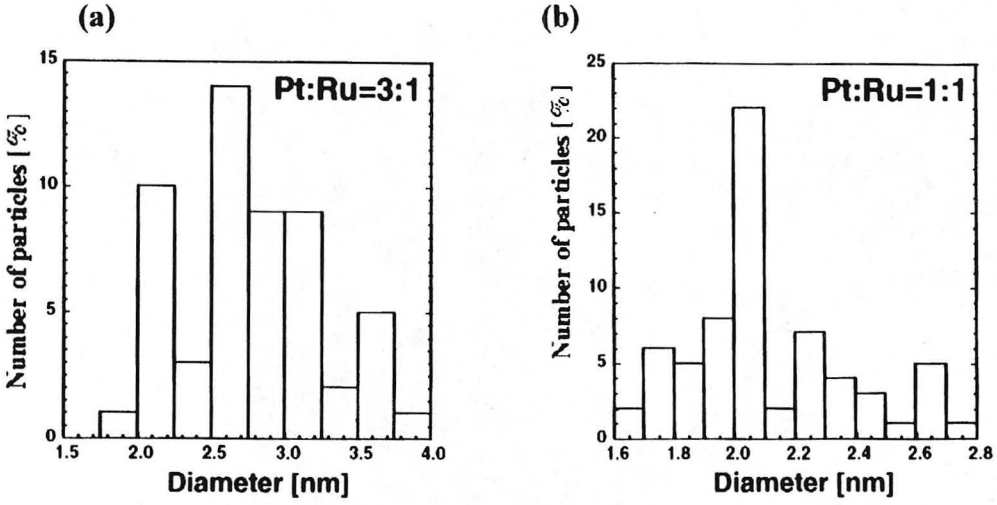

Radmilivić *et al*, Figure 5

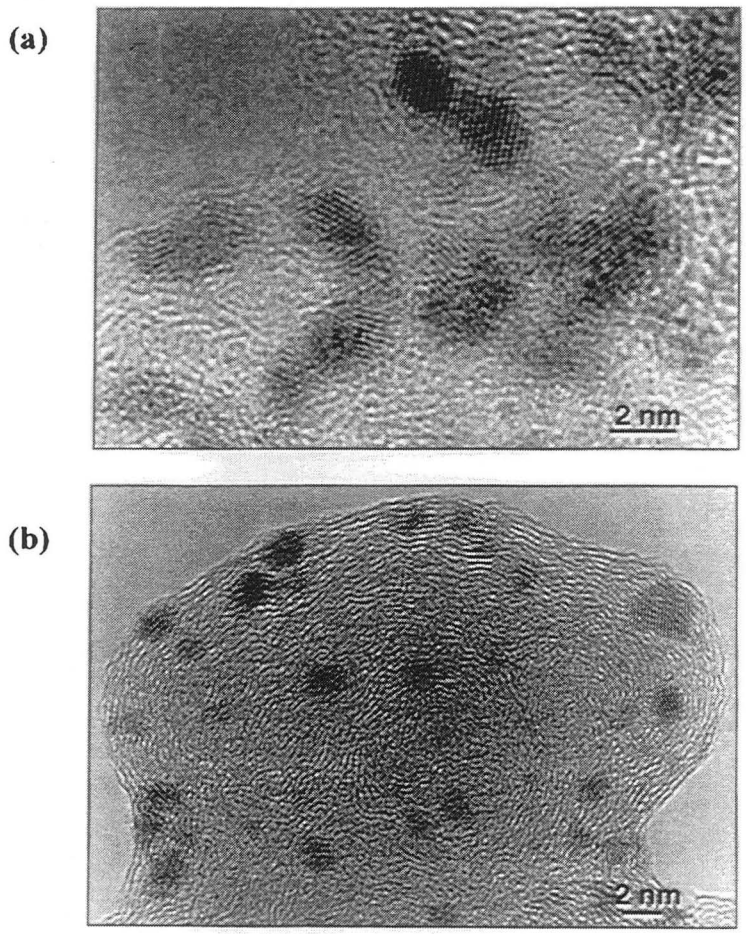

Radmilović *et al.* Figure 6

(a) (b)

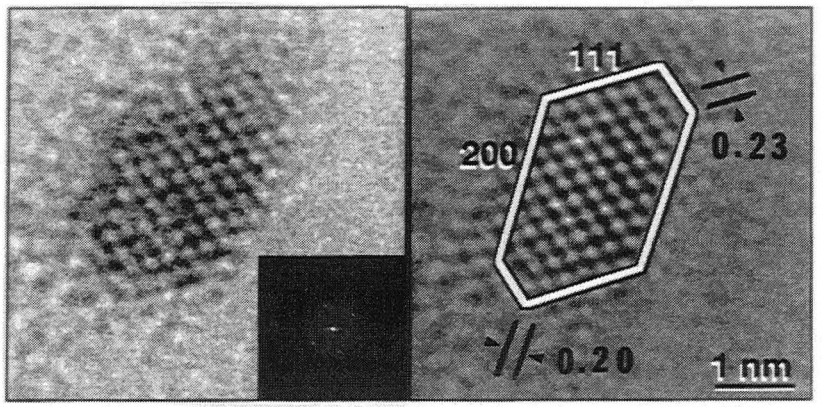

Radmilović *et al*. Figure 7

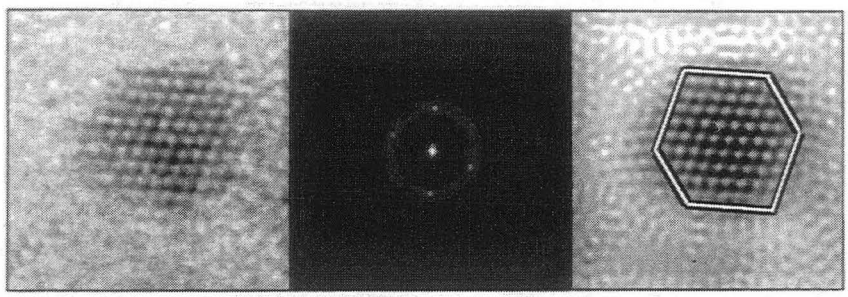

Radmilović *et al*. Figure 8

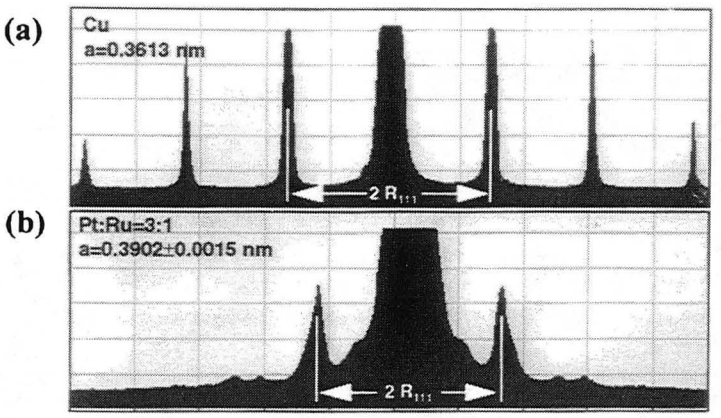

Radmilović *et al*. Figure 9

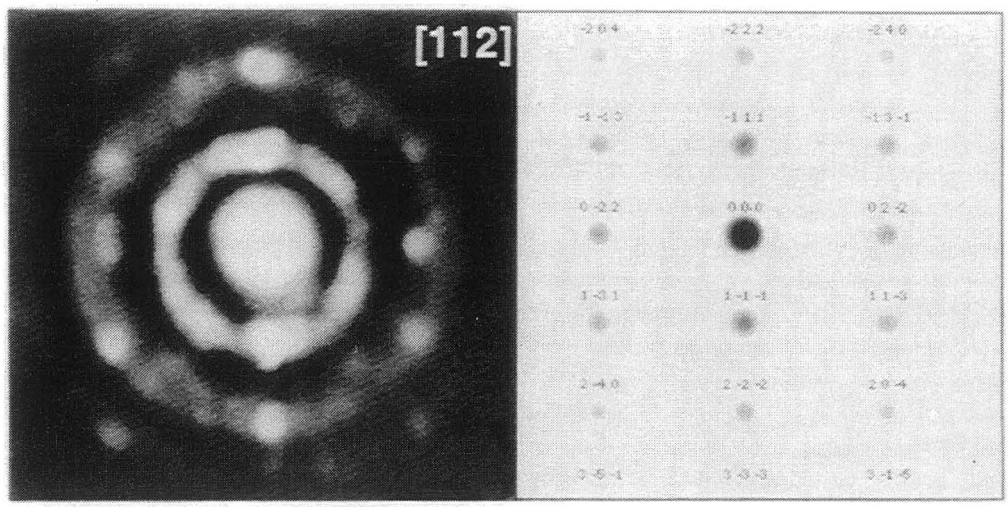

Radmilović *et al*. Figure 10

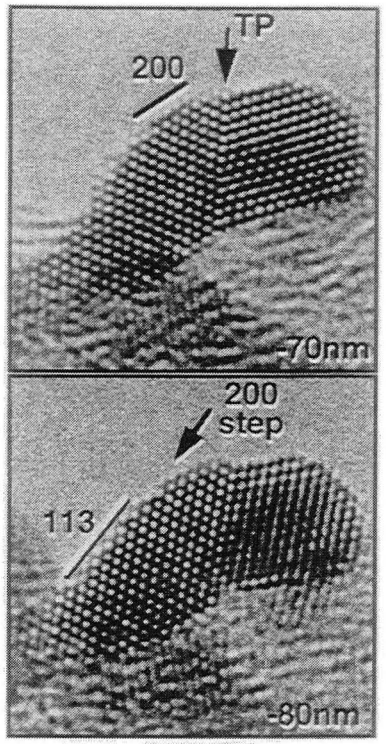

Radmilović *et al.* Figure 11

LAWRENCE BERKELEY LABORATORY
UNIVERSITY OF CALIFORNIA
TECHNICAL INFORMATION DEPARTMENT
BERKELEY, CALIFORNIA 94720